# A novel tool for dynamic cell adhesion studies – the De-Adhesion Number Investigator DANI

**Andreas Hartmann, Melanie E. M. Stamp, Ralf Kmeth, Sascha Buchegger, Bernd Stritzker, Belma Saldamli, Rainer Burgkart, Matthias F. Schneider, Achim Wixforth**

# A novel tool for dynamic cell adhesion studies – the De-Adhesion Number Investigator DANI

Andreas Hartmann,[abe] Melanie Stamp,[ae] Ralf Kmeth,[c] Sascha Buchegger,[c] Bernd Stritzker,[c] Belma Saldamli,[d] Rainer Burgkart,[d] Matthias F. Schneider[b] and Achim Wixforth*[ae]

For an optimal implementation of materials, such as, *e.g.* medical implants in living environments, a thorough characterization of cell adhesion, kinetics and strength is required, as well as a prerequisite *e.g.* for bone integration. Here we present a miniaturized (~100 μl) lab-on-a-chip implant hybrid system which allows quantification of cell adhesion under dynamic conditions mimicking those of physiological relevance. Surface acoustic waves are excited and used on optical transparent chips to induce micro acoustic streaming and to create a microfluidic shear spectrum ranging from 0 to ~35 s$^{-1}$. We demonstrate its potential for a time-efficient, dynamic screening test of new implant materials using a model of an osseointegration with SAOS-2 cells. The upside-down orientation also allows utilization of the micro reactor on non-transparent materials like titanium and diamond-like-carbon (DLC).

## Introduction

Apart from fundamental scientific interest, the study of cell adhesion in general and the evaluation of the properties of different cell–material-combinations are crucial for medical purposes. Examples are osseointegration of endoprostheses as total hip replacements and others, where fast and lasting adhesion of osteogenic cells is required, or stents, that ideally completely prevent cell adhesion. A presently and commonly used approach in this research area is the spinning disc method, where cells are grown on a substrate and kept in a culture medium, and a disc is rotated over them at a given distance (*cf.* ref. 1) leading to a shear force field. A typical, quantitative measure in these experiments is the distance to the center of rotation, where 50% of the cells are detached. This allows for the calculation of the corresponding force acting on the cells. An inherent problem of this method, however, is the fact that it usually only allows the observation of the initial and final state, but no dynamic, live observation of the ongoing experiment. Another common setup for probing cell adhesion is flow chambers (*cf.* ref. 2). These are usually driven by syringe pumps. Therefore, they necessarily require an open system with large amounts of lab consumables and significant dead volumes.

Meanwhile, a well-established alternative way to handle small amounts of fluids for various applications is based on the "acoustic streaming" effect due to surface acoustic waves (SAW) excited on piezo-electric materials (*cf.* ref. 3–6 and 16–20). Recently, in the framework of our group, this technology was translated to closed chamber systems (*cf.* ref. 7–10).

One of their major advantages is the possibility to realize closed μ-chambers of only a few tens of microliters which results in very low sample volumes needed. Moreover, as we employ optical transparent piezo-electric materials like LiNbO$_3$, the experiments allow for live video observation of the experiment while they are operating.

The particular system realized and described here is a very versatile tool for implant research under physiological conditions. It is capable of modeling and investigating the dynamic initial cell adhesion processes of arbitrary cell–material-combinations with little need of cells (60k) as well as small sized implant material (disc with $r$ = 5 mm, $h$ = 2 mm). Thereby, it has the potential of being a time- and cost-efficient, highly functional screening method for systematic optimization of functionalized implant surfaces. From a biological view point, it allows for live optical observation and inspection of cells being exposed to a shear spectrum induced by the microfluidic flow field. Therefore, the presented system holds great potential of becoming a valuable tool in implant research as it states a simple and cheap method that closes

[a] *Experimental Physics I, University of Augsburg, 86159 Augsburg, Germany. E-mail: achim.wixforth@physik.uni-augsburg.de*
[b] *Dept. of Mechanical Engineering, Boston University, Boston, Massachusetts, USA*
[c] *Experimental Physics IV, University of Augsburg, 86159 Augsburg, Germany*
[d] *Clinic of Orthopaedic Surgery, Klinikum rechts der Isar, Technical University of Munich, Germany*
[e] *Nanosystems Initiative Munich NIM, Schellingstrasse 4, 80799 Munich, Germany*

an existing gap in adhesion studies that is present due to the lack of appropriate methods so far.

## Materials and methods

### Surface acoustic wave-driven flow system

For the generation of the microfluidic flow, Ti–Ag–Ti (5 nm by 50 nm by 5 nm height) inter-digital transducers (IDT) on a substrate of $LiNbO_3$ (128° rot Y-cut) with a resonance frequency at ~160 MHz were fabricated and used to excite surface acoustic waves. To protect the IDT, a $SiO_2$ coating was sputter deposited on top of the IDT structures. The $LiNbO_3$ substrate at the same time represents the bottom of our micro flow chamber. For a detailed description of the SAW excitation employing IDT, see ref. 11.

On top of the piezoelectric substrate with the IDT, a hollow, cylindrical polydimethylsiloxane (PDMS) structure (outer diameter 16 mm, inner diameter 8 mm, height 2 mm) constitutes the wall of the chamber which contains only about 100 µl volume. On top of this guard ring, the implant sample is placed into a small pocket formed by the PDMS structure as well (see Fig. 1). The chamber is then surrounded by a hollow brass body which is coupled to a heat bath ensuring body temperature (37 °C) in the chamber. Thus, SAW mediated



Fig. 1 Photograph (top) and schematic cross-section (bottom) of the setup for cell adhesion measurements. The system consists of a transparent piezoelectric $LiNbO_3$ substrate with interdigital transducers (IDTs, green-brown color in the figure). On top of the substrate and the IDTs, a polydimethylsiloxane (PDMS)-chamber (blue) is placed which is covered by the implant specimen, in this case a titanium sample (grey). In the top photograph, the PDMS-chamber (upside-down) is removed from the $LiNbO_3$ substrate, whereas the cross-section in the bottom part of the figure shows the system in its closed and assembled configuration. The electrical radio-frequency (rf) connector is labeled in orange. It is connected to the IDTs *via* silver conductive paste and two separated Cu-parts on the chip-carrier.

heating effects are compensated, and we can ensure a constant temperature within the flow chamber throughout the entire experiment.

The measurements are performed using an Axiovert 200 M (Zeiss) inverted microscope, a 2.5× objective and a digital camera (Hamamatsu Orca 5G) with 1344 × 1024 pixels. This results in an observable area of 3.48 × 2.65 $mm^2$. The SAW driven microfluidic flow is created using a frequency generator powering the IDTs at their resonance frequency with an input power of up to +27 dBm (= 500 mW). Employing particle image velocimetry (PIV) (*cf.* ref. 12, PIVlab-code by Dipl. Biol. William Thielicke and Prof. Dr. Eize J. Stamhuis), we are able to obtain the distribution of the shear rates in the chamber. For visualization purposes, we use small ($d$ = 6 microns) tracer particles (Polybeads® from Polyscience Inc., Warrington, PA).
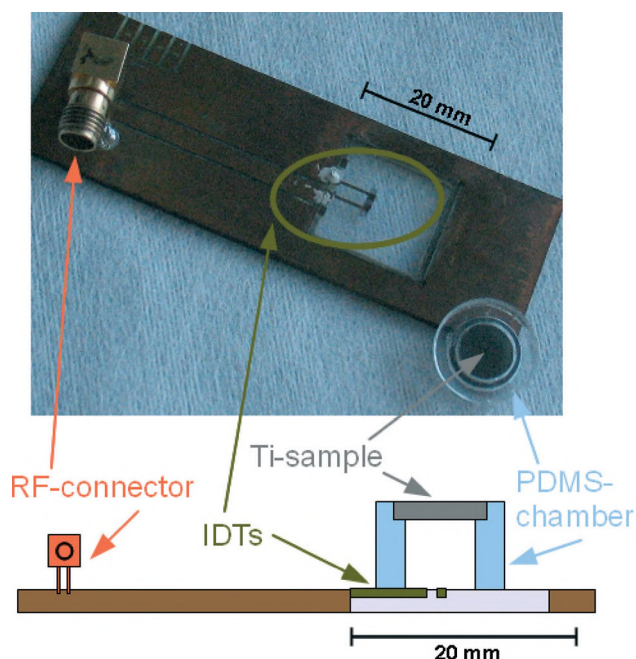
### Cell culture

The SAOS-2 cell line was provided by Klinikum rechts der Isar, Technical University of Munich, TUM. It was cultured using DMEM medium with stable glutamine, 3.7 g $l^{-1}$ $NaHCO_3$, 1.0 g $l^{-1}$ D-glucose (Biochrom) adding 50 ml fetal calf serum (FBS Superior, S 0615, Biochrom), 10 ml HEPES 1 M (L 1613, Biochrom), 5 ml L-glutamine 200 mM (K 0283, Biochrom), 5 ml MEM vitamins 100× (K 0373, Biochrom), and 1 ml primocin (ant-pm-2, Invivogen) in a humidified atmosphere consisting of 5% $CO_2$ and 95% air at 37 °C. Cells could take up nutrients *ad libitum*.

### Implant samples

The medical titanium alloy (Ti gr.5-ELI) material was purchased from Valbruna Edel Inox GmbH, Dormagen, Germany. The samples (discs with $r$ = 5 mm, $h$ = 2 mm) were sand blasted by Aesculap AG, Tuttlingen, Germany, which resulted in a surface roughness Ra of ~5 µm. Further on, they were cleaned for 20 minutes in an ultrasonic bath at 50 °C in a solution of 1 : 1 acetone–isopropanol. Finally, they were sterilized in an autoclave at 121 °C for 20 minutes. Alternatively, we also produced DLC-covered implant samples according to ref. 13, except that the molar ratios were changed to 1 : 2 benzoin : $AgNO_3$ and $AgNO_3$ : polyvinylpyrrolidone (PVP) to four different concentrations of 1 : 2, 1 : 10, 1 : 20 and pure PVP. The use of silver in the first three leads to the formation of silver nanoparticles in the DLC matrix, with Ag concentration being dependent on the Ag : PVP ratio. These particles have been introduced for antibacterial reasons. This is especially important during the first days after surgery. All DLC-samples were sterilized according to medical standards using a cobalt 60-source (1.1732 MeV and 1.3325 MeV) with a radiation dose of 26.5 kGy.

### Image processing

To deduce the number of cells on the substrate as a function of time, the images were analyzed using the software "ImageJ" provided by the NIH. As the cells occurred mostly in agglomerations, the identified particles were sorted into

10 bins of different areas that were heuristically defined starting at 100 μm$^2$ (which corresponds to a circle of radius $r = 5.64$ μm) up to 5000 μm$^2$ ($r = 39.89$ μm). The bins were interrelated to 1–10 cells.

## Results and discussion

### Shear field distribution in the measuring chamber

The force counteracting the cell adhesion originates from the shear stress created near the wall/implant material sample. Using the velocity field as being extracted from our PIV measurements, we calculated the corresponding shear stress distribution in the $x$–$y$-plane of the substrate.

The shear rates in the observable area for cell adhesion measurements range from 0 to ~35 s$^{-1}$ (*cf.* Fig. 2). Due to the characteristic streaming pattern of our IDT-structure (*cf.* ref. 14 and 15), a half-moon-shaped pattern of high shear rates with two distinct maxima is developing on the sample after the SAW is turned on. The amplitude of these shear rates can easily be adjusted by adjusting the rf power fed into the IDT.

### Preparation procedure

After harvesting the cells, a cell suspension (in medium) is prepared with a density of approx. 360k cells ml$^{-1}$. The cells are stained with 1 μl of calcein green AM fluorescent dye (Invitrogen, 1 μg dissolved in 1 μl dimethyl sulfoxide) per ml of suspension for $t > 30$ min. This also serves as a valuable viability proof, as only after removal of the acetoxymethyl (AM) esters by intracellular esterases is the molecule converted to a green fluorescent dye. 160 μl (approx. 60k cells) are loaded into the chamber, initially forming a dome due to surface tension. The sample is then stored in the incubator for different periods of time (incubation time $t\_inc$: typically 10 min $< t\_inc < 60$ min) where the cell sediment ($t\_sed < 1$ min for cells with a radius of 10 μm following a Stokes' law estimate) start to adhere to the surface. After this initial adhesion time, the medium above the sample is gently exchanged by pipetting at a very low speed. Basically no suspended cells remain present in the measuring chamber at the initial state of the measurement. After further 15 minutes of preparation ($t\_prep$), the cells are exposed to the microfluidic flow by switching on the SAW and subsequent micro acoustic streaming.

### Adhesion study of SAOS-2 cells

We now demonstrate the potential of our setup to investigate the adhesion of osteoblast-related SAOS-2 cells on titanium surfaces at 37 °C. In Fig. 3, we depict the result of such an experiment by plotting the increasing total number of adhered cells with increasing initial adhesion time. In this example, we observe a total number of about 1200 seeded cells mm$^{-2}$.

In Fig. 4, we show the evolution of cell de-adhesion within the first 60 minutes of implant sample shear treatment by

**Fig. 3** Number of adhered SAOS-2 cells mm$^{-2}$ on naked titanium after an initial adhesion time of $t\_inc$ (10–60 min) in the incubator at standard cell culture conditions; 1.2k cells mm$^{-2}$ were seeded.
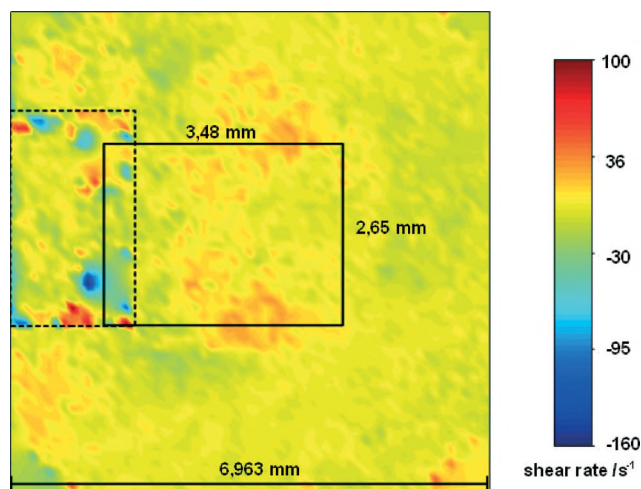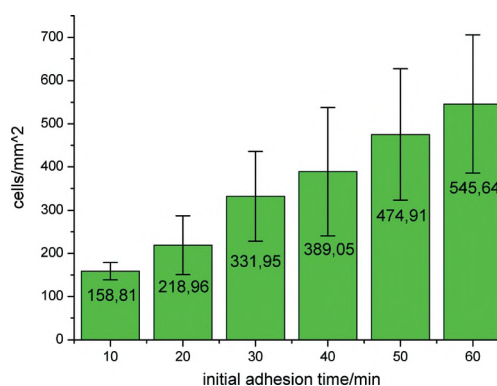
**Fig. 2** Shear rate distribution within the measuring chamber; the viewing area for cell adhesion measurements is marked by a continuous black rectangle. Shear rates range from 0 to ~35 s$^{-1}$ and create a typical pattern with two areas of maximum shear rates with a saddle point area in between, reflecting the typical IDT streaming characteristics. The dotted rectangle marks the position of the IDT; the apparent distinct minima and maxima in this area are caused by computational artifacts due to the lack of sight of tracer particles and therefore have no physical meaning.

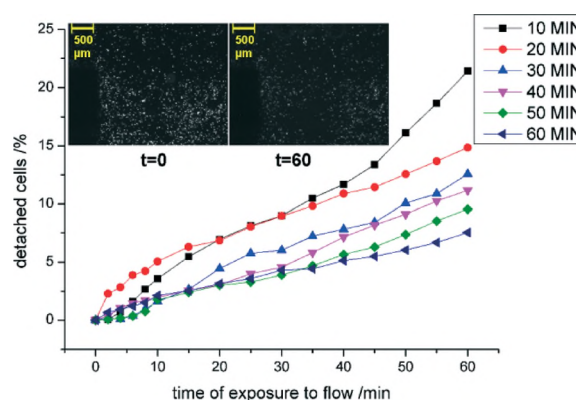**Fig. 4** Percentage of detached SAOS-2 cells on Ti-implant samples depending on initial adhesion time $t\_inc$ (10–60 min) *versus* time of flow exposure. It can be clearly seen that for higher initial adhesion times, the detachment rate of the cells due to the microfluidic flow is reduced. The photograph insets exemplarily depict the initial and final cell density within the measuring chamber.

the microfluidic flow for six different initial adhesion times (ranging from 10 to 60 minutes). The data clearly show that the initial adhesion time and the average detachment rate are inversely related.

An alternative and different adhesion study is performed with SAOS-2 cells on titanium samples covered with a layer of diamond-like-carbon (DLC), which is also known to be a very suitable implant surface material. The DLC matrices were either pure or doped with nano-colloidal silver particles (*cf.* sample preparation-part). Fig. 5 depicts a comparison of the initial adhesion affinity for three different DLC coatings and pure titanium. On titanium, we clearly observe a higher cell density after $t\_inc = 60$ min whereas the DLC coated samples reveal a slightly increased adhesion affinity for higher silver-doping concentrations among the Ag–PVP 1 : 10 and Ag–PVP 1 : 20 samples. Nonetheless, it is important to state that for a very high silver-doping (Ag–PVP 1 : 2), no cells at all were bound to the surface after $t\_inc = 60$ min. Although the well-documented cell toxicity of silver gives a plausible explanation for the lack of cells for Ag–PVP 1 : 2, we are not aware of a stringent explanation for the increased cell affinity for the slightly higher silver-doping of Ag–PVP 1 : 10 as compared to Ag–PVP 1 : 20. A positive, electrostatic potential due to silver ions in the DLC matrix close to the surface should in principle be shielded very effectively by a Gouy–Chapman layer as the Debye-length in a cell culture medium is significantly below 1 nm. Still, it seems worth mentioning that a positively charged surface represents a quite unusual condition in a biological system which might have unexpected effects.

The dynamic cell adhesion measurements under microfluidic flow, in contrast, give another impression of the suitability of the different materials for cell adhesion. Fig. 6 shows the de-adhesion of SAOS-2 cells with respect to the different implant surfaces. Apart from titanium, which exhibits the highest initial adhesion density and the lowest de-adhesion rate, the DLC implant samples show a different behavior: the Ag : PVP 1 : 10 sample with the highest initial adhesion density among the DLC samples surprisingly also turns out to exhibit the largest de-adhesion rate. With decreasing silver concentration (Ag : PVP 1 : 20 to pure DLC), the de-adhesion rate also decreases.
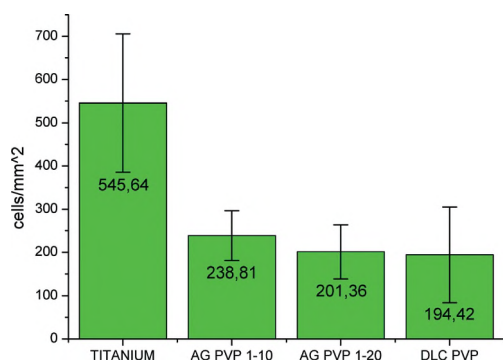


**Fig. 5** Number of adhered SAOS-2 cells mm$^{-2}$ on various substrates as being denoted on the *x*-axis. The data were taken after an initial adhesion time of $t\_inc = 60$ min in the incubator under standard cell culture conditions; 1.2k cells mm$^{-2}$ were seeded.
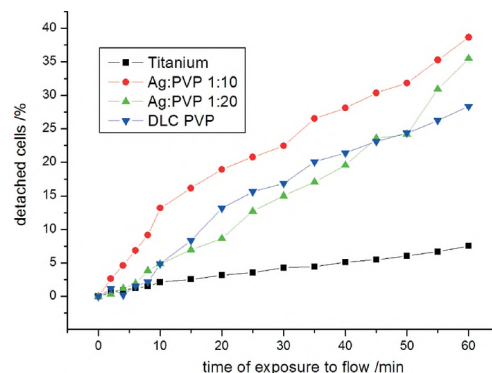


**Fig. 6** Percentage of detached SAOS-2 cells on different samples as marked by different symbols after 60 minutes of initial adhesion time *versus* time of flow exposure. Titanium exhibits the smallest de-adhesion rate as compared to the different DLC surfaces. Within this set of substrates, the de-adhesion tendency increases with higher silver-doping.

Whatever might be the reason for the higher initial cell affinity of Ag–PVP 1 : 10 compared to Ag–PVP 1 : 20, the dynamic de-adhesion behavior could be well explained by the cytotoxicity of the silver ions harming the cell and ultimately killing it.

From this described procedure, we can derive 2 relevant parameters for implant research: the initial adhesion affinity and the de-adhesion rate. The presented results indicate that both parameters can be independent of each other as for example titanium had the highest initial adhesion affinity and the lowest de-adhesion rate, whereas within the (populated) DLC-samples, the sample with the highest initial adhesion affinity (Ag : PVP 1 : 10) also showed the largest de-adhesion rate. Interestingly, even small differences of the adhesion/de-adhesion behavior can be resolved despite the small volume of the chamber. This is a consequence of the heterogeneous shear stress profile (Fig. 2), which at first glance may be regarded as a shortcoming of our chamber geometry. The high sensitivity of the PIV measurements, however, over-compensates this shortcoming by far and provides a whole spectrum of shear rates in one single setup to which the cells are exposed to. Thereby the setup provides an important feature of a time-efficient screening test, analyzing the effect of different shear rates on a single view.

## Conclusions

A new tool for the quantitative, dynamic analysis of cell adhesion and detachment has been developed. The tool stands out through its extremely small sample volume, short measuring times and high flexibility, allowing investigation of the adhesion properties of any substrate, irrespective of its optical (*e.g.* transparency), mechanical (*e.g.* roughness or hardness) or electrical properties. This was achieved by employing SAW driven microfluidics in an upside-down orientation. Measuring times are strongly reduced by creating an entire shear spectrum within a single experiment, which is analyzed using PIV. The design of the system enables the operator to easily vary the measuring parameters (like *e.g.* temperature,

pH or chemical changed environments) which makes it very versatile to probe cell adhesion under controlled physiological as well as pathological conditions. The economic operation of the system is demonstrated for the study of implant compatibility. To extend the applicability to stent research, the shear rates need to be further increased. We currently approach this problem by changing the IDT geometry and/or by increasing the number of IDTs on a single chip.

## Acknowledgements

## Notes and references

1 L. Weiss, The measurement of cell adhesion *Exp. Cell Res.*, 1961, **153**, 141–153.

2 S. Usami, H. H. Chen, Y. Zhao, S. Chien and R. Skalak, Design and construction of a linear shear stress flow chamber *Ann. Biomed. Eng.*, 1993, **21**(1), 77–83.

3 S. Shiokawa, Y. Matsui and T. Ueda, Liquid streaming and droplet formation caused by leaky Rayleigh waves *Proc. - IEEE Ultrason. Symp.*, 1989, 643–646.

4 A. Wixforth, C. J. Strobl, C. Gauer, A. Tögl, J. Scriba and Z. V. Guttenberg, Acoustic Manipulation of Small Droplets *Anal. Bioanal. Chem.*, 2004, **379**, 982–991.

5 A. Wixforth, Acoustically Driven Planar Microfluidics *Superlattices Microstruct.*, 2004, **33**, 389.

6 S. W. Schneider, S. Nuschele, A. Wixforth, C. Gorzelanny, A. Alexander-Katz, R. R. Netz and M. F. Schneider, Shear-induced unfolding triggers adhesion of von Willebrand factor fibers *Proc. Natl. Acad. Sci. U. S. A.*, 2007, **104**(19), 7899–7903.

7 K. Sritharan, C. J. Strobl, M. F. Schneider, A. Wixforth and Z. V. Guttenberg, Acoustic Mixing at Low Reynold's Numbers *Appl. Phys. Lett.*, 2006, **88**, 054102.

8 C. Fillafer, G. Ratzinger, J. Neumann, Z. Guttenberg, S. Dissauer, I. K. Lichtscheidl, M. Wirth, F. Gabor and M. F. Schneider, An acoustically-driven biochip – impact of flow on the cell-association of targeted drug carriers *Lab Chip*, 2009, **9**, 2782–2788.

9 M. A. Fallah, V. M. Myles, T. Krüger, K. Sritharan, A. Wixforth, F. Varnik, S. W. Schneider and M. F. Schneider, Acoustic driven flow and lattice Boltzmann simulations to study cell adhesion in biofunctionalized-microfluidic channels with complex geometry *Biomicrofluidics*, 2010, **4**, 024106.

10 L. Schmid, A. Wixforth, D. A. Weitz and T. Franke, Novel surface acoustic wave (SAW)-driven closed PDMS flow chamber *Microfluid. Nanofluid.*, 2012, **12**(1–4), 229–235.

11 R. M. White and F. W. Voltmer, Direct Piezoelectric Coupling To Surface Elastic Waves *Appl. Phys. Lett.*, 1965, **7**(12), 314.

12 R. Lindken, M. Rossi, S. Grosse and J. Westerweel, Micro-Particle Image Velocimetry (microPIV): recent developments, applications, and guidelines *Lab Chip*, 2009, **9**, 2551–2567.

13 F. P. Schwarz, I. Hauser-Gerspach, T. Waltimo and B. Stritzker, Antibacterial properties of silver containing diamond like carbon coatings produced by ion induced polymer densification *Surf. Coat. Technol.*, 2011, **205**(20), 4850–4854.

14 Z. V. Guttenberg, A. Rathgeber, S. Keller, J. O. Rädler, A. Wixforth, M. Kostur, M. Schindler and P. Talkner, Flow Profiling of a Surface Acoustic Wave Nanopump *Phys. Rev. E: Stat., Nonlinear, Soft Matter Phys.*, 2004, **70**, 056311.

15 T. Frommelt, M. Kostur, P. Talkner and P. Hanggi, Flow Patterns and Transport in Rayleigh Surface Acoustic Wave Streaming: Combined Finite Element Method and Raytracing Numerics versus Experiments *IEEE Trans. Ultrason. Ferroelectr. Freq. Control*, 2008, **55**(10), 2298–2305.

16 X. Ding, P. Li, S.-C. S. Lin, Z. S. Stratton, N. Nama, F. Guo, D. Slotcavage, X. Mao, J. Shi, F. Costanzo and T. J. Huang, Surface acoustic wave microfluidics *Lab Chip*, 2013, **13**(18), 3626–3649.

17 X. Ding, S.-C. S. Lin, B. Kiraly, H. Yue, S. Li, I.-K. Chiang, J. Shi, S. J. Benkovic and T. J. Huang, On-chip manipulation of single microparticles, cells, and organisms using surface acoustic waves *Proc. Natl. Acad. Sci. U. S. A.*, 2012, **109**(28), 11105–11109.

18 J. Friend and L. Y. Yeo, Microscale acoustofluidics: Microfluidics driven via acoustics and ultrasonics *Rev. Mod. Phys.*, 2011, **83**(2), 647–704.

19 H. Li, J. Friend, L. Yeo, A. Dasvarma and K. Traianedes, Effect of surface acoustic waves on the viability, proliferation and differentiation of primary osteoblast-like cells *Biomicrofluidics*, 2009, **3**(3), 34102.

20 H. Li, J. R. Friend and L. Y. Yeo, A scaffold cell seeding method driven by surface acoustic waves *Biomaterials*, 2007, **28**(28), 4098–4104.